**Mechanics
&
Industry**

REGULAR ARTICLE

OPEN ◈ ACCESS

Disturbance rejection control with H_∞ optimized observer for vibration suppression of piezoelectric smart structures

Xiao-Yu Zhang[1], Shun-Qi Zhang[2,*], Zhan-Xi Wang[1], Xian-Sheng Qin[1], Run-Xiao Wang[1], and Rüdiger Schmidt[3]

[1] School of Mechanical Engineering, Northwestern Polytechnical University, West Youyi Street 127, 710072 Xi'an, PR China
[2] School of Mechatronic Engineering and Automation, Shanghai University, Shangda Road 99, 200444 Shanghai, PR China
[3] Institute of Structural Mechanics and Lightweight Design, RWTH Aachen University, Wüllnerstraße 7, 52062 Aachen, Germany

Abstract. In this paper, a disturbance rejection (DR) control with H_∞ optimized observer is developed for vibration suppression of smart structures considering model uncertainties and measurement noise. An electromechanically coupled dynamic finite element (FE) model of piezoelectric smart structures is firstly built for control design. Based on the dynamic FE model, the H_∞ optimized observer is designed with a dynamic feedback gain which is calculated by H_∞ mixed sensitivity optimization. Expected response speed and robustness to model uncertainties and measurement noise are obtained by configuring proper weighting functions. In the closed-loop system, estimated disturbances and state variables are fed back through a conventional DR controller to counteract disturbances and stabilize the system. In order to validate the DR control with H_∞ optimized observer, vibration suppression simulations of a piezoelectric smart beam are implemented in the absence and presence of model uncertainties and measurement noise, respectively. Furthermore, DR control with generalized proportional integral observer and DR control with high-gain proportional integral observer are added for comparison. Results show that excellent vibration suppression performance and better robustness to model uncertainties and measurement noise are achieved by the DR control with H_∞ optimized observer.

Keywords: Disturbance rejection control / H_∞ mixed sensitivity optimization / smart structures / vibration suppression

1 Introduction

Due to the increasing demand of energy saving, light weight structures are widely applied in the fields of aerospace and automotive engineering. However, some light weight structures are very sensitive to dynamic disturbances because of their low stiffnesses and damping ratios, which leads to unwanted vibrations. To achieve better human comfort, mechanical performance and reliability, many vibration suppression technologies were developed by researchers in the past few decades [1–3]. As an active vibration suppression system, piezoelectric smart structure has advantages such as excellent electromechanical coupling property, wide frequency response, easy processing and bonding nature. Therefore, the application of piezoelectric smart structures in the field of active vibration suppression has attracted the interest of many researchers.

As a matter of fact, the design of control methods plays a very important role in the active vibration suppression systems. In the field of vibration suppression of piezoelectric smart structures, many types of control schemes have been proposed and developed during the past few decades. For example, traditional control methods like negative velocity feedback control [4–6], positive position feedback control [7–10], PID control [11–14] and bang–bang control [15–17]; modern control methods such as Lyapunov control [18,19], linear quadratic regulator (LQR) control [18,20–22] and linear quadratic Gaussian (LQG) control [20,23–26]. There are also some advanced control and intelligent control methods which can be found in the literature, for instance, sliding model control [27,28], model predictive control [29,30], fuzzy logic control [31,32] and neural network control [33–35]. Nevertheless, these control methods cannot suppress vibrations very efficiently because external disturbances are not considered in the design of these control methods, which are exactly the major cause of vibrations. In most of these control strategies, only states or outputs are fed back in most

* e-mail: zhangsq@shu.edu.cn

closed-loop systems, it is enough for system stabilization, but not the most efficient way to suppress vibrations.

Since most vibrations are caused by external disturbances, one efficient way to largely suppress vibrations is to acquire the disturbance model or signal and use it to dissipate the vibrations in the closed-loop system. Two typical control methods are feedforward control and disturbance rejection (DR) control [36]. The feedforward control feeds disturbance signals to the feedforward controller to compensate real disturbances, which works perfectly when the disturbances are known or can be measured directly by sensors. However, the feedforward control cannot be applied to the practical problems in which the disturbances are unknown and unmeasurable. On the other hand, the DR control shows advantages in such situations because known disturbances or accurately measured disturbance signals are not necessary for the DR control. Instead, it estimates disturbances through a specific observer and feeds the estimated disturbances to the controller, which leads to counteraction of the influence of disturbances and efficient vibration suppression.

In the literature of control engineering, there are several different types of DR control. Han [37] developed active disturbance rejection control (ADRC) for single-input single-output systems. Li et al. applied ADRC to piezoelectric multi-mode vibration control for a stiffened plate numerically and experimentally [38,39]. But there is still no mature design method for the nonlinear feedback gains of ADRC, which makes it difficult to calculate proper gain parameters for expected system performance. Based on ADRC, Gao [40] developed a linear feedback strategy, which is called linear active disturbance rejection control (LADRC). Excellent DR performance can be obtained by configuring high observer gains in LADRC. However, the side effect of a high-gain observer is the sensitivity to measurement noise, which limits the practical applications of LADRC, to a certain degree. For multi-input multi-output systems, Müller and Lückel [41] proposed and developed a DR control with proportional-integral (PI) observer, which estimates disturbances and feeds the estimated signals back to the system through a DR controller. In the framework of DR control, the PI observer was extended to a generalized proportional-integral (GPI) observer and then applied to vibration suppression of smart structures by Zhang et al. [42,43]. With known disturbance frequencies, the GPI observer is capable to estimate disturbances very accurately and the DR control with GPI observer can suppress vibrations of smart structures perfectly. Nevertheless, system robustness to model uncertainties and measurement noise is not considered in the aforementioned DR control methods, which cannot be neglected in practical problems and may result in unstable closed-loop systems.

In order to achieve better vibration suppression performance for smart structures, and keep the control system robust to model uncertainties and measurement noise in the mean time, a DR control with H_∞ optimized observer is proposed and developed in this paper. In the proposed method, H_∞ mixed sensitivity optimization is adopted to calculate the dynamic feedback gain of the observer. The H_∞ optimized observer can obtain expected response speed and robustness to model uncertainties and measurement noise through selecting proper weighting functions. In such a way, disturbances can be estimated accurately and better counteracted in the closed-loop systems which suffer model uncertainties or measurement noise. Through vibration suppression simulations of a piezoelectric smart beam, the DR control with H_∞ optimized observer is validated and compared with DR control with GPI observer and DR control with high-gain PI observer, considering additive model uncertainty and measurement noise, respectively. The simulation results indicate that the DR control with H_∞ optimized observer has excellent vibration suppression performance and better robustness to model uncertainties and measurement noise.

2 System modeling

2.1 Constitutive equations

For the piezoelectric materials, due to the assumption of small strain and weak electric field, linear constitutive equations are considered as

$$\boldsymbol{\sigma} = \mathbf{c}\boldsymbol{\varepsilon} - \mathbf{e}^{\mathrm{T}}\mathbf{E}, \tag{1}$$

$$\mathbf{D} = \mathbf{e}\boldsymbol{\varepsilon} + \boldsymbol{\epsilon}\mathbf{E} \tag{2}$$

with

$$\mathbf{e} = \mathbf{d}\mathbf{c}. \tag{3}$$

In the above equations, $\boldsymbol{\sigma}$, $\boldsymbol{\varepsilon}$, $\mathbf{E}$ and $\mathbf{D}$ denote the stress vector, the strain vector, the electric field vector and the electric displacement vector, respectively. Matrices $\mathbf{c}$, $\boldsymbol{\epsilon}$ and $\mathbf{d}$ represent the elasticity constant matrix, the dielectric constant matrix and the piezoelectric constant matrix, respectively. Since the electric field considered here is relatively week, the electric potential is assumed to be linearly distributed through the piezoelectric materials. The value of electric field can be calculated by

$$\mathbf{E} = -\mathrm{grad}\,\boldsymbol{\phi} = \mathbf{B}_\phi \boldsymbol{\phi} \tag{4}$$

where $\boldsymbol{\phi}$ is the electric potential, grad denotes the gradient operation and $\mathbf{B}_\phi$ is the electric field matrix.

2.2 Dynamic model

Plate and shell structures are the most common light weight structures, and also the typical type of smart structures considered in this paper. In small deformation situations, the geometrically linear first-order shear deformation (FOSD) hypothesis is capable to describe the strain-displacement relations. Applying Hamilton's principle and finite element (FE) method, the dynamic FE model of smart structures is obtained as [44–46]

$$\mathbf{M}_{uu}\ddot{\mathbf{q}} + \mathbf{C}_{uu}\dot{\mathbf{q}} + \mathbf{K}_{uu}\mathbf{q} + \mathbf{K}_{u\phi}\boldsymbol{\phi}_a = \mathbf{f}, \tag{5}$$

$$\mathbf{K}_{\phi u}\mathbf{q} + \mathbf{K}_{\phi\phi}\boldsymbol{\phi}_s = \mathbf{0}. \tag{6}$$

Equations (5) and (6) are respectively the motion equation and sensor equation, in which matrices $\mathbf{M}_{uu}$, $\mathbf{C}_{uu}$, $\mathbf{K}_{uu}$, $\mathbf{K}_{u\phi}$, $\mathbf{K}_{\phi u}$ and $\mathbf{K}_{\phi\phi}$ denote the mass matrix, the damping matrix, the stiffness matrix, the piezoelectric coupled stiffness matrix, the coupled capacity matrix and the piezoelectric capacity matrix, respectively. Vectors $\mathbf{q}$, $\boldsymbol{\phi}_a$, $\mathbf{f}$ and $\boldsymbol{\phi}_s$ represent the nodal displacement vector, the actuation voltage vector, the external force vector and the sensor voltage vector, respectively.

2.3 State space model

In order to build a state space model for control design, the state vector $\mathbf{x}$, input vector $\mathbf{u}$, measured output vector $\mathbf{y}$ and controlled output vector $\mathbf{z}$ are firstly defined as

$$\mathbf{x} = \left\{ \begin{array}{c} \mathbf{q} \\ \dot{\mathbf{q}} \end{array} \right\}, \mathbf{u} = \boldsymbol{\phi}_a, \mathbf{y} = \boldsymbol{\phi}_s + \mathbf{n}, \mathbf{z} = \boldsymbol{\phi}_s \qquad (7)$$

where $\mathbf{n}$ is the measurement noise vector. Subsequently, based on the dynamic FE model given in equations (5) and (6), the state space model of smart structures is obtained as

$$\dot{\mathbf{x}}(t) = \mathbf{A}\mathbf{x} + \mathbf{B}\mathbf{u} + \mathbf{N}\mathbf{f}, \qquad (8)$$

$$\mathbf{y}(t) = \mathbf{C}_1\mathbf{x} + \mathbf{D}_1\mathbf{u} + \mathbf{n}, \qquad (9)$$

$$\mathbf{z}(t) = \mathbf{C}_2\mathbf{x} + \mathbf{D}_2\mathbf{u} \qquad (10)$$

where $\mathbf{A}$, $\mathbf{B}$, $\mathbf{N}$, $\mathbf{C}_1$, $\mathbf{D}_1$, $\mathbf{C}_2$ and $\mathbf{D}_2$ denote the system matrix, the control input matrix, the disturbance input matrix, the measured system output matrix, the measured output feed-through matrix, the controlled system output matrix and the controlled output feed-through matrix, respectively. The matrices above are calculated by

$$\mathbf{A} = \begin{bmatrix} \mathbf{0} & \mathbf{I} \\ -\mathbf{M}_{uu}^{-1}\mathbf{K}_{uu} & -\mathbf{M}_{uu}^{-1}\mathbf{C}_{uu} \end{bmatrix}, \qquad (11)$$

$$\mathbf{B} = \begin{bmatrix} \mathbf{0} \\ -\mathbf{M}_{uu}^{-1}\mathbf{K}_{u\phi} \end{bmatrix}, \qquad (12)$$

$$\mathbf{N} = \begin{bmatrix} \mathbf{0} \\ \mathbf{M}_{uu}^{-1} \end{bmatrix}, \qquad (13)$$

$$\mathbf{C}_1 = \mathbf{C}_2 = \begin{bmatrix} -\mathbf{K}_{\phi\phi}^{-1}\mathbf{K}_{\phi u} & \mathbf{0} \end{bmatrix}, \qquad (14)$$

$$\mathbf{D}_1 = \mathbf{D}_2 = \mathbf{0}. \qquad (15)$$

In order to describe the system with model uncertainties, the transfer function of the system in equations (8) and (9) is defined as

$$\mathbf{G}(s) = \mathbf{C}_1(s\mathbf{I} - \mathbf{A})^{-1}\mathbf{B} + \mathbf{D}_1 \qquad (16)$$

where $\mathbf{G}(s)$ is the transfer function, s denotes the complex variable. Common model uncertainties like parameter
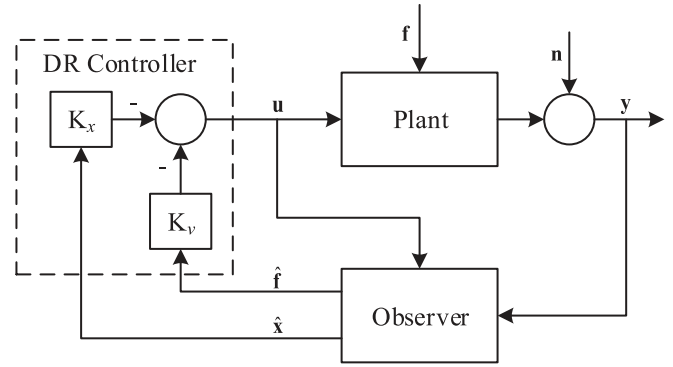

Fig. 1. The schematic diagram of DR control system.

perturbation and unmodeled dynamics can be described by additive uncertainty. Therefore, the system with model uncertainties can be described by

$$\mathbf{G}_{\mathrm{u}}(s) = \mathbf{G}(s) + \Delta_{\mathrm{a}}(s) \qquad (17)$$

where $\mathbf{G}_{\mathrm{u}}(s)$ and $\Delta_{\mathrm{a}}(s)$ represent the transfer function of system with model uncertainties and the transfer function of additive uncertainty, respectively.

3 Disturbance rejection control with H_∞ optimized observer

To get a better comprehension of DR control, a schematic diagram of DR control is given in Figure 1 to show the working mechanism of DR control system. The core idea of DR control is to counteract disturbances by feeding estimated disturbances back to the system. For that reason, firstly, disturbances and state variables of the plant are estimated through a specific observer, as shown in Figure 1. Thereafter the estimated state vector $\hat{\mathbf{x}}$ and the estimated disturbance vector $\hat{\mathbf{f}}$ are fed back to the system with properly designed control gains $\mathbf{K}_x$ and $\mathbf{K}_v$, which leads to a stable closed-loop system and disturbance counteraction. Therefore, the DR control needs not only a stable controller to stabilize the system, but also an observer with fast convergence speed to supply accurately estimated disturbances.

3.1 Fictitious disturbance model

Generally speaking, most observers are designed for observing system state variables but not disturbances. Therefore, the external disturbances are approximated by state variables of a fictitious disturbance model first, which is expressed as

$$\mathbf{f}(t) = \mathbf{H}\mathbf{v}(t) + \Delta_{\mathrm{r}}(t), \qquad (18)$$

$$\dot{\mathbf{v}}(t) = \mathbf{V}\mathbf{v}(t). \qquad (19)$$

It can be seen that the linear relation between vectors $\mathbf{f}$ and $\mathbf{v}$ is described by matrix $\mathbf{H}$, and the dynamic characteristic

of vector $\mathbf{v}$ is described by matrix $\mathbf{V}$. Vector $\boldsymbol{\Delta}_r$ represents the residual error between the real disturbance $\mathbf{f}$ and linear part $\mathbf{Hv}$. The residual error $\boldsymbol{\Delta}_r$ is assumed to be small and can be neglected.

When choosing the fictitious disturbance model, the dynamic information of real disturbances should be involved in the disturbance model if it is known. The reason is that the dynamic characteristics of the disturbance model have great influence on the disturbance tracking performance of the observer, especially for disturbances with similar dynamic characteristics. Therefore, a fictitious disturbance model containing disturbance frequency information is adopted in this paper. This fictitious disturbance model was firstly used in the GPI observer [42,43], in which disturbances are approximated by combinations of constant terms and cosine terms. For example, the ith disturbance f_i can be approximated by

$$f_i \approx a_{i0} + a_{i1}\cos(\omega_i t) \qquad (20)$$

where ω_i can be given by the disturbance frequency. If there is only one disturbance applied on the smart structure, vector $\mathbf{v}$ and matrices $\mathbf{H}$, $\mathbf{V}$ can be obtained as

$$\mathbf{v} = \left\{ \begin{array}{c} a_{10} \\ a_{11}\cos(\omega_1 t) \\ a_{11}\sin(\omega_1 t) \end{array} \right\}, \qquad (21)$$

$$\mathbf{H} = [\, 1 \quad 1 \quad 0 \,], \qquad (22)$$

$$\mathbf{V} = \begin{bmatrix} 0 & 0 & 0 \\ 0 & 0 & -\omega_1 \\ 0 & \omega_1 & 0 \end{bmatrix}. \qquad (23)$$

3.2 Observer design

3.2.1 Extended system

In order to estimate disturbances through an observer, the system needs to be extended with the fictitious state variables. Substituting equations (18) and (19) into equations (8)–(10) yields an extended system as

$$\left\{ \begin{array}{c} \dot{\mathbf{x}} \\ \dot{\mathbf{v}} \end{array} \right\} = \mathbf{A}_e \left\{ \begin{array}{c} \mathbf{x} \\ \mathbf{v} \end{array} \right\} + \mathbf{B}_e \mathbf{u} + \begin{bmatrix} \mathbf{N} \\ \mathbf{0} \end{bmatrix} \boldsymbol{\Delta}_r, \qquad (24)$$

$$\mathbf{y} = \mathbf{C}_e \left\{ \begin{array}{c} \mathbf{x} \\ \mathbf{v} \end{array} \right\} + \mathbf{D}_e \mathbf{u} + \mathbf{n} \qquad (25)$$

where matrices $\mathbf{A}_e$, $\mathbf{B}_e$, $\mathbf{C}_e$ and $\mathbf{D}_e$ denote the system matrix, the control input matrix, the measured system output matrix and the measured output feed-through matrix, respectively. The matrices in equations (24) and (25) can be calculated by

$$\mathbf{A}_e = \begin{bmatrix} \mathbf{A} & \mathbf{NH} \\ \mathbf{0} & \mathbf{V} \end{bmatrix}, \qquad (26)$$
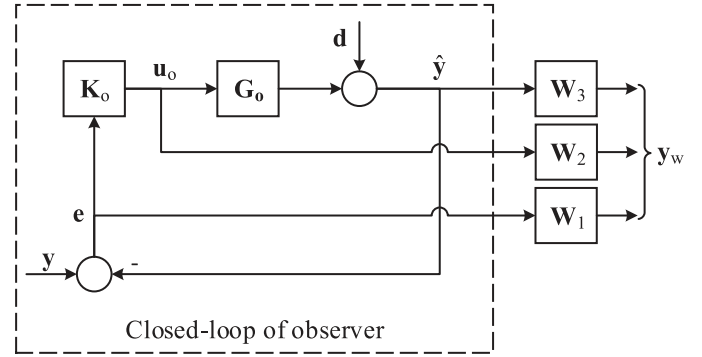

Fig. 2. The H_∞ mixed sensitivity tracking control problem of observer.

$$\mathbf{B}_e = \begin{bmatrix} \mathbf{B} \\ \mathbf{0} \end{bmatrix}, \qquad (27)$$

$$\mathbf{C}_e = [\, \mathbf{C} \quad \mathbf{0} \,], \qquad (28)$$

$$\mathbf{D}_e = \mathbf{0}. \qquad (29)$$

According to the structure of Luenberger observer, one obtains an observer for the extended system as

$$\left\{ \begin{array}{c} \dot{\hat{\mathbf{x}}} \\ \dot{\hat{\mathbf{v}}} \end{array} \right\} = \mathbf{A}_e \left\{ \begin{array}{c} \hat{\mathbf{x}} \\ \hat{\mathbf{v}} \end{array} \right\} + \mathbf{B}_e \mathbf{u} + \mathbf{K}_o(\mathbf{y} - \hat{\mathbf{y}}), \qquad (30)$$

$$\hat{\mathbf{y}} = \mathbf{C}_e \left\{ \begin{array}{c} \hat{\mathbf{x}} \\ \hat{\mathbf{v}} \end{array} \right\} + \mathbf{D}_e \mathbf{u} \qquad (31)$$

where $\hat{\mathbf{x}}$, $\hat{\mathbf{v}}$, $\hat{\mathbf{y}}$ are the estimated values of $\mathbf{x}$, $\mathbf{v}$, $\mathbf{y}$, respectively. The feedback gain $\mathbf{K}_o$ can be static or dynamic, as long as it can stabilize the observer system, which leads to the convergence of $\hat{\mathbf{x}}$, $\hat{\mathbf{v}}$, $\hat{\mathbf{y}}$.

3.2.2 Dynamic feedback design

To achieve excellent control performance for DR control, the observer needs not only convergence but also fast responding speed, which means accurate and rapid estimation of disturbances and state variables. Simultaneously, the observer is also required to be robust to measurement noise and model uncertainties which exist extensively in practical applications. In this paper, H_∞ mixed sensitivity optimization is used to design the dynamic feedback gain $\mathbf{K}_o$. The observer system in equations (30) and (31) can be regarded as an H_∞ mixed sensitivity tracking control problem depicted in Figure 2, in which $\mathbf{G}_o$ is the controlled observer system. Vectors $\mathbf{e}$, $\mathbf{u}_o$, $\mathbf{d}$, $\mathbf{n}$ and $\mathbf{y}_w$ denote the tracking error vector, the feedback input vector, the output disturbance vector, the measurement noise vector and the weighted output vector, respectively. Furthermore, $\mathbf{W}_1$, $\mathbf{W}_2$ and $\mathbf{W}_3$ are the weighting functions of the signals in $\mathbf{y}_w$. The transfer function of $\mathbf{G}_o$ is expressed as

$$\mathbf{G}_{\mathrm{o}}(s) = \mathbf{C}_{\mathrm{e}}(s\mathbf{I} - \mathbf{A}_{\mathrm{e}})^{-1}\mathbf{B}_{\mathrm{e}} + \mathbf{D}_{\mathrm{e}}. \tag{32}$$

Accordingly, the open-loop transfer function from $\mathbf{y}$ to $\hat{\mathbf{y}}$ is obtained as

$$\mathbf{L}(s) = \mathbf{G}_{\mathrm{o}}(s)\mathbf{K}_{\mathrm{o}}(s). \tag{33}$$

The closed-loop transfer functions from $\mathbf{y}$ to $\mathbf{e}$, $\mathbf{u}$ and $\hat{\mathbf{y}}$, are calculated by

$$\mathbf{S}(s) = (\mathbf{I} + \mathbf{L}(s))^{-1}, \tag{34}$$

$$\mathbf{R}(s) = \mathbf{K}_{\mathrm{o}}(s)(\mathbf{I} + \mathbf{L}(s))^{-1}, \tag{35}$$

$$\mathbf{T}(s) = \mathbf{I} - \mathbf{S}(s) \tag{36}$$

where $\mathbf{S}(s)$ and $\mathbf{T}(s)$ are usually called sensitivity function and complementary sensitivity function of the system, respectively. Since $\mathbf{R}(s)$ is the transfer function from the reference input to the feedback input, the feedback effort can be measured by $\mathbf{R}(s)$. The sensitivity function $\mathbf{S}(s)$ also represents the closed-loop transfer function from $\mathbf{d}$ to $\hat{\mathbf{y}}$, which means that a smaller gain of $\mathbf{S}(s)$ would result in better tracking performance and smaller influence of output disturbances on system outputs. On the other hand, the complementary sensitivity function $\mathbf{T}(s)$ is the closed-loop transfer function from $\mathbf{n}$ to $\hat{\mathbf{y}}$, hence measurement noises can be attenuated in the closed-loop system if the gain of $\mathbf{T}(s)$ is small enough. However, $\mathbf{S}(s)$ and $\mathbf{T}(s)$ cannot be simultaneously small at the same frequency because they are complementary functions to each other. Therefore, to achieve desired tracking performance and robustness, trade-offs have to be made between the conflicting goals in different frequency ranges. One simple way is setting proper weighting functions to shape $\mathbf{S}(s)$ and $\mathbf{T}(s)$ as

$$\bar{\sigma}(\mathbf{S}(\mathrm{j}\omega)) \leq \bar{\sigma}(\mathbf{W}_1^{-1}(\mathrm{j}\omega)), \tag{37}$$

$$\bar{\sigma}(\mathbf{T}(\mathrm{j}\omega)) \leq \bar{\sigma}(\mathbf{W}_3^{-1}(\mathrm{j}\omega)) \tag{38}$$

where $\bar{\sigma}$ represents the maximum singular value. Moreover, for robust stability in the presence of model uncertainties like parameter perturbation and unmodeled dynamics, etc., which can be represented by additive model uncertainty, $\bar{\sigma}(\mathbf{R}(\mathrm{j}\omega))$ should be made small, i.e.,

$$\bar{\sigma}(\mathbf{R}(\mathrm{j}\omega)) \leq \bar{\sigma}(\mathbf{W}_2^{-1}(\mathrm{j}\omega)). \tag{39}$$

Then the dynamic controller $\mathbf{K}_{\mathrm{o}}$ can be derived by solving an H_∞ optimal problem expressed as

$$\min\gamma, \mathrm{s.t.} \parallel \mathbf{P}(s) \parallel_\infty < \gamma \tag{40}$$

where γ is the performance index, $\mathbf{P}(s)$ is the weighted system expressed as

$$\mathbf{P}(s) = \begin{bmatrix} \mathbf{W}_1\mathbf{S}(s) \\ \mathbf{W}_2\mathbf{R}(s) \\ \mathbf{W}_3\mathbf{T}(s) \end{bmatrix}. \tag{41}$$

The H_∞ optimal problem can be solved by the two Riccati equations [47]. According to the transfer function $\mathbf{P}(s)$, the state space model of $\mathbf{P}$ can be obtained as

$$\mathbf{P} = \begin{bmatrix} \bar{\mathbf{A}} & \bar{\mathbf{B}}_1 & \bar{\mathbf{B}}_2 \\ \bar{\mathbf{C}}_1 & \bar{\mathbf{D}}_{11} & \bar{\mathbf{D}}_{12} \\ \bar{\mathbf{C}}_2 & \bar{\mathbf{D}}_{21} & \bar{\mathbf{D}}_{22} \end{bmatrix}. \tag{42}$$

For detailed calculation of the matrices in equation (42), one can refer to [48]. Solving the two Riccati equations expressed as

$$\bar{\mathbf{A}}^{\mathrm{T}}\mathbf{X} + \mathbf{X}\bar{\mathbf{A}} + \mathbf{X}(\gamma^2\bar{\mathbf{B}}_1\bar{\mathbf{B}}_1^{\mathrm{T}} - \bar{\mathbf{B}}_2\bar{\mathbf{B}}_2^{\mathrm{T}})\mathbf{X} + \bar{\mathbf{C}}_1\bar{\mathbf{C}}_1^{\mathrm{T}} = 0, \tag{43}$$

$$\bar{\mathbf{A}}\mathbf{Y} + \mathbf{Y}\bar{\mathbf{A}}^{\mathrm{T}} + \mathbf{Y}(\gamma^2\bar{\mathbf{C}}_1^{\mathrm{T}}\bar{\mathbf{C}}_1 - \bar{\mathbf{C}}_2^{\mathrm{T}}\bar{\mathbf{C}}_2)\mathbf{Y} + \bar{\mathbf{B}}_1^{\mathrm{T}}\bar{\mathbf{B}}_1 = 0, \tag{44}$$

one yields the state space model of controller $\mathbf{K}_{\mathrm{o}}$ as

$$\dot{\mathbf{x}}_{\mathrm{k}} = \mathbf{A}_\infty\mathbf{x}_{\mathrm{k}} - \mathbf{Z}_\infty\mathbf{L}_\infty\mathbf{u}_{\mathrm{k}}, \tag{45}$$

$$\mathbf{y}_{\mathrm{k}} = \mathbf{F}_\infty\mathbf{x}_{\mathrm{k}} \tag{46}$$

where

$$\mathbf{A}_\infty = \bar{\mathbf{A}} + \gamma^{-2}\bar{\mathbf{B}}_1\bar{\mathbf{B}}_1^T\mathbf{X} + \bar{\mathbf{B}}_2\mathbf{F}_\infty + \mathbf{Z}_\infty\mathbf{L}_\infty\bar{\mathbf{C}}_2, \tag{47}$$

$$\mathbf{F}_\infty = -\bar{\mathbf{B}}_2^{\mathrm{T}}\mathbf{X}, \tag{48}$$

$$\mathbf{L}_\infty = -\mathbf{Y}\bar{\mathbf{C}}_2^{\mathrm{T}}, \tag{49}$$

$$\mathbf{Z}_\infty = (\mathbf{I} - \gamma^{-2}\mathbf{Y}\mathbf{X})^{-1}. \tag{50}$$

3.3 Controller design

As described before, the estimated disturbances and state variables need to be fed back to the system to counteract disturbances and stabilize the system, through a DR controller with the control law defined as

$$\mathbf{u} = -\mathbf{K}_x\hat{\mathbf{x}} - \mathbf{K}_v\hat{\mathbf{v}} \tag{51}$$

where $\mathbf{K}_x$ and $\mathbf{K}_v$ denote the feedback gain matrices for $\hat{\mathbf{x}}$ and $\hat{\mathbf{v}}$, respectively. To construct a stable closed-loop system, the state feedback gain $\mathbf{K}_x$ can be designed by many methods such as LQR, pole placement method, H_∞ optimization, etc. Considering the convenience of comparisons with other DR control methods in later simulations, LQR is employed in this paper, which is also used in the DR control with PI observer and DR
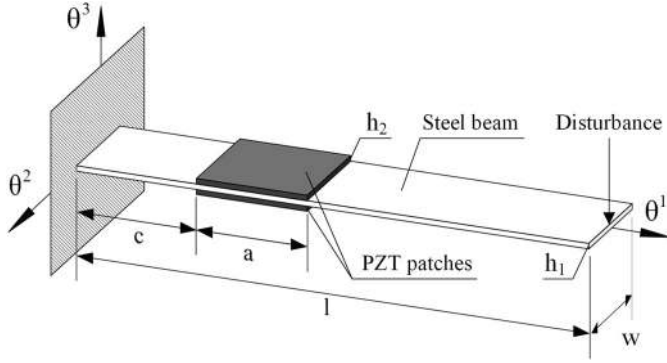
Fig. 3. Cantilevered smart beam bonded with piezoelectric patches.

control with GPI observer [42,43]. The feedback gain $\mathbf{K}_x$ is calculated by

$$\mathbf{K}_x = \mathbf{R}_\mathrm{r}^{-1}\mathbf{B}^\mathrm{T}\mathbf{P}\mathbf{x} \tag{52}$$

where the symmetric positive definite matrix $\mathbf{P}$ can be obtained by solving an algebraic Riccati equation expressed as

$$\mathbf{A}^\mathrm{T}\mathbf{P} + \mathbf{P}\mathbf{A} + \mathbf{Q}_\mathrm{r} - \mathbf{P}\mathbf{B}\mathbf{R}_\mathrm{r}^{-1}\mathbf{B}^\mathrm{T}\mathbf{P} = 0 \tag{53}$$

with

$$\mathbf{Q}_\mathrm{r} = \mathbf{C}^\mathrm{T}\mathbf{Q}\mathbf{C}, \mathbf{R}_\mathrm{r} = \mathbf{R}. \tag{54}$$

The symmetric positive definite matrices $\mathbf{Q}$ and $\mathbf{R}$ are the weighting matrices that penalize the system output and system input signals, respectively, which can be approximated by Bryson's rule [49].

For disturbance counteraction, the feedback gain $\mathbf{K}_v$ can be designed by assuming a linear relation between $\mathbf{x}$ and $\mathbf{v}$ [43] as

$$\mathbf{x} = \mathbf{X}_v\mathbf{v} \tag{55}$$

where $\mathbf{X}_v$ is the linear mapping matrix. Considering equation (19), one obtains

$$\dot{\mathbf{x}} = \mathbf{X}_v\dot{\mathbf{v}} = \mathbf{X}_v\mathbf{V}\mathbf{v}. \tag{56}$$

Substituting equations (51), (55) and (56) into the state space model (8) and (10) and assuming the controlled output $\mathbf{z}$ as zero, one obtains

$$(\mathbf{A} - \mathbf{B}\mathbf{K}_x)\mathbf{X}_v - \mathbf{X}_v\mathbf{V} - \mathbf{B}\mathbf{K}_v + \mathbf{N}\mathbf{H} = 0, \tag{57}$$

$$(\mathbf{C}_2 - \mathbf{D}_2\mathbf{K}_x)\mathbf{X}_v - \mathbf{D}_2\mathbf{K}_v = 0. \tag{58}$$

Table 1. Geometrical data of the steel beam and piezoceramic patches.

Steel beam	Piezoceramic patches
$l = 350\,\mathrm{mm}$	$a = 75\ \mathrm{mm}$
$w = 25\,\mathrm{mm}$	$c = 50\,\mathrm{mm}$
$h_1 = 0.8\,\mathrm{mm}$	$h_2 = 0.25\,\mathrm{mm}$

Considering the matrices $\mathbf{X}$, $\mathbf{K}_v$ and $\mathbf{H}$ are constituted of three parts as

$$\mathbf{X} = [\,\mathbf{X}_1 \quad \mathbf{X}_2 \quad \mathbf{X}_3\,], \tag{59}$$

$$\mathbf{K}_v = [\,\mathbf{K}_{v1} \quad \mathbf{K}_{v2} \quad \mathbf{K}_{v3}\,], \tag{60}$$

$$\mathbf{H} = [\,\mathbf{H}_1 \quad \mathbf{H}_2 \quad \mathbf{H}_3\,], \tag{61}$$

meanwhile, substituting equations (22), (23) into equations (57) and (58), one obtains

Then $\mathbf{K}_v$ can be derived by solving equation (62).

## 4 Vibration suppression simulation

4.1 Simulation model

To validate the proposed DR control with H_∞ optimized observer, a cantilevered smart beam bonded with two collocated piezoceramic patches is employed for numerical simulations of vibration suppression, as pictured in Figure 3. The polarization directions of the two piezoceramic patches are opposite along the θ^3 axis, hence the two patches can function as an actuator and a sensor, respectively. A concentrated disturbance force is applied at the tip node of the smart beam, in the direction of axis θ^3. The specific geometrical and material data of the smart beam can be found in Tables 1 and 2, respectively.

The electromechanically coupled FE model of the smart beam is built using a 14×1 mesh and eight-node serendipity shell elements with quadratic shape functions. As shown in Figure 4a, the smart beam is modeled by 14 shell elements with a size of $25\,\mathrm{mm} \times 25\,\mathrm{mm}$ each. The shell elements are placed in the mid-surface of the smart beam and arranged in line along the beam. The steel beam and PZT patches are regarded as different material layers of the shell elements. Integrals along the thickness direction are calculated separately in each layer when computing the

$$\begin{bmatrix} \mathbf{A} - \mathbf{B}\mathbf{K}_x & \mathbf{0} & \mathbf{0} & -\mathbf{B} & \mathbf{0} & \mathbf{0} \\ \mathbf{0} & \mathbf{A} - \mathbf{B}\mathbf{K}_x & -\omega_1\mathbf{I} & \mathbf{0} & -\mathbf{B} & \mathbf{0} \\ \mathbf{0} & \omega_1\mathbf{I} & \mathbf{A} - \mathbf{B}\mathbf{K}_x & \mathbf{0} & \mathbf{0} & -\mathbf{B} \\ \mathbf{C}_2 - \mathbf{D}_2\mathbf{K}_x & \mathbf{0} & \mathbf{0} & -\mathbf{D}_2 & \mathbf{0} & \mathbf{0} \\ \mathbf{0} & \mathbf{C}_2 - \mathbf{D}_2\mathbf{K}_x & \mathbf{0} & \mathbf{0} & -\mathbf{D}_2 & \mathbf{0} \\ \mathbf{0} & \mathbf{0} & \mathbf{C}_2 - \mathbf{D}_2\mathbf{K}_x & \mathbf{0} & \mathbf{0} & -\mathbf{D}_2 \end{bmatrix} \begin{bmatrix} \mathbf{X}_1 \\ \mathbf{X}_2 \\ \mathbf{X}_3 \\ \mathbf{K}_{v1} \\ \mathbf{K}_{v2} \\ \mathbf{K}_{v3} \end{bmatrix} = \begin{bmatrix} -\mathbf{N}\mathbf{H}_1 \\ -\mathbf{N}\mathbf{H}_2 \\ -\mathbf{N}\mathbf{H}_3 \\ \mathbf{0} \\ \mathbf{0} \\ \mathbf{0} \end{bmatrix}. \tag{62}$$

Table 2. Material data of the steel beam and piezoceramic patches.

Property	Symbol	Steel beam	Piezoceramic patches
Young's modulus (GPa)	Y	210	67
Density (kg/m³)	ρ	7900	7800
Poisson's ratio	v	0.3	0.3
Piezoelectric coefficient (C/N)	d_{31}, d_{32}	–	-2.1×10^{-10}
Permittivity (F/m)	ϵ_{33}	–	2.13×10^{-8}
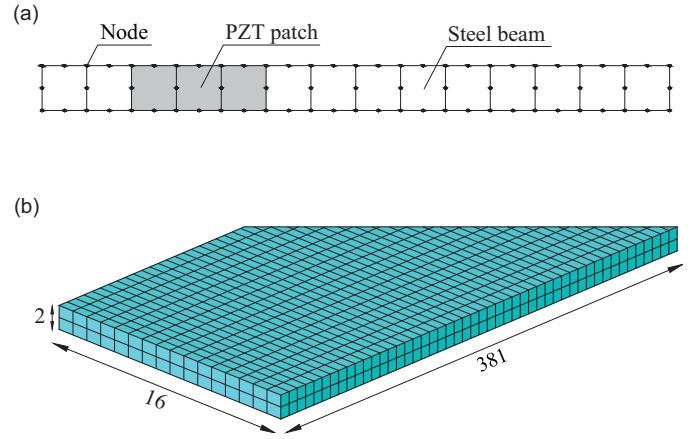
Fig. 4. Mesh details of the smart beam: (a) mesh of 14×1 shell elements, (b) mesh of $381 \times 16 \times 2$ solid elements.

Table 3. Eigenfrequencies of the first five bending modes of the smart beam (Hz).

Mesh	Element	Mode 1	Mode 2	Mode 3	Mode 4	Mode 5	Maximal error
14×1	Shell	6.0672	33.2706	95.0806	190.5112	312.7494	0.08%
$257 \times 11 \times 1$	Solid	6.0735	33.302	95.115	190.57	312.61	0.04%
$314 \times 13 \times 1$	Solid	6.0730	33.299	95.109	190.55	312.58	0.03%
$381 \times 16 \times 2$	Solid	6.0711	33.291	95.088	190.51	312.50	–

stiffness and mass matrices. To avoid the membrane and shear locking problems, uniformly reduced integration scheme is employed in the integral calculations. Since the shell thickness does not change during deformation in the FOSD hypothesis, and the electric field through the thickness is assumed as constant, the electric field in the PZT material can be regarded as a uniform field. The dynamic model is coded and calculated in Matlab, and so are the following vibration control algorithms and simulations.

To satisfy the equivalent of the Nyquist criteria in mesh design, i.e. at least six elements per wavelength are necessary to detect the corresponding modal frequency [50,51], the mesh density and model accuracy must be evaluated. For the smart beam with fixed-free boundary condition, the first five bending modes in θ^3 direction consist of, in turn, one quarter, three quarters, one and a quarter, one and three quarters, two and a quarter of a structural wavelength. Clearly, the 14×1 mesh fulfills the above criteria for the first five bending modes in θ^3 direction. To verify the accuracy of the FE model with 14×1 mesh, a reference model of the smart beam is built and analyzed in ANSYS. The FE model in ANSYS is constituted of 14144 hexahedral solid elements with quadratic shape functions, including the elements of the steel beam and PZT patches. As shown in Figure 4b, the numbers of elements in three dimensions of the steel beam are $381 \times 16 \times 2$. Through modal analysis in ANSYS, the modal information of the smart beam is obtained. Besides,

to test the convergency of the $381 \times 16 \times 2$ mesh, the smart beam is also analyzed in ANSYS using $257 \times 11 \times 1$ and $314 \times 13 \times 1$ meshes. Eigenfrequencies of the first five bending modes of the smart beam with four different meshes are listed in Table 3. Regarding the model with $381 \times 16 \times 2$ mesh as a reference, the maximum errors of the five eigenfrequencies of the models with other meshes are calculated and listed in Table 3. For the models analyzed in ANSYS, it can be seen from Table 3 that both the maximum errors of the five eigenfrequencies of models with $257 \times 11 \times 1$ and $314 \times 13 \times 1$ meshes are less than 0.05%, therefore the $381 \times 16 \times 2$ mesh is believed to be convergent. The error of the five eigenfrequencies of model with 14×1 mesh is 0.08%. Considering the first eigenfrequency of the smart beam is the highest vibration frequency simulated in this paper; therefore, the mesh density and model accuracy satisfy the requirements of the following simulations.

4.2 Simulation results
4.2.1 Vibration suppression with model uncertainties

The two simulations in this section are implemented considering additive model uncertainty and harmonic disturbances with different frequencies, which are 2π rad/s and the first eigenfrequency of the smart beam, respectively. Furthermore, DR control with GPI observer is also applied in these two simulations for comparison. Since the LQR is employed in both the DR control with H_∞
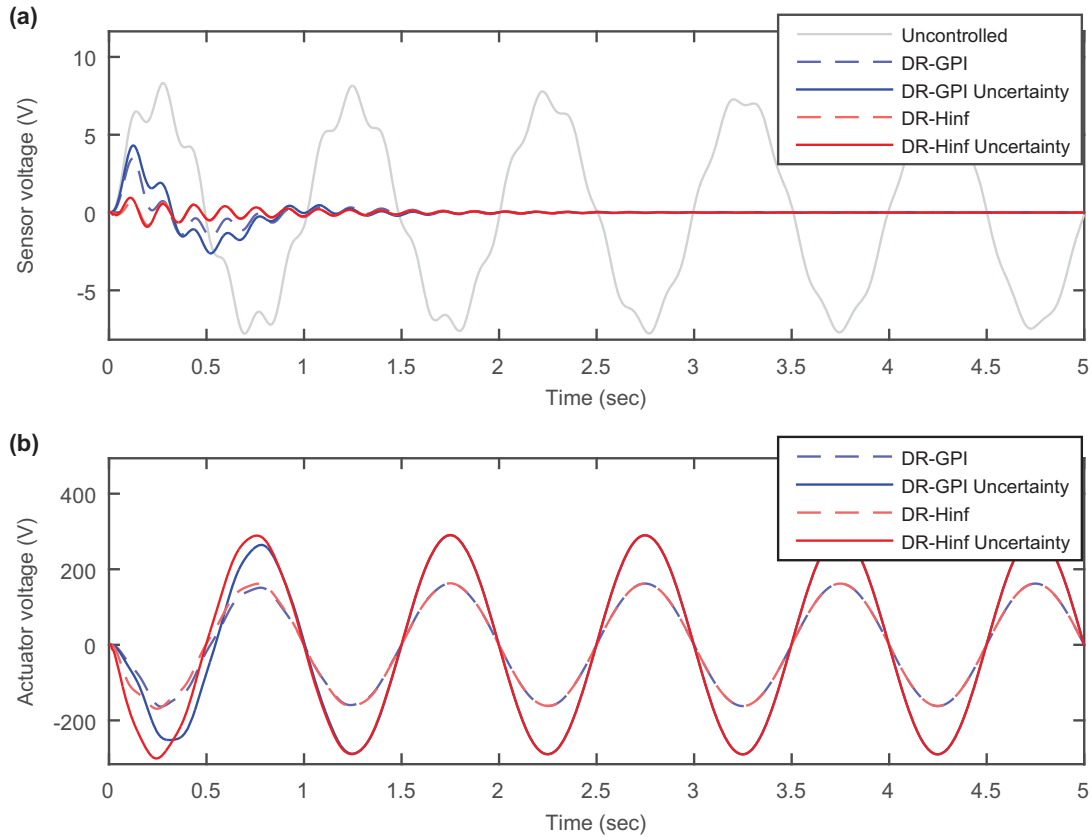
Fig. 5. The vibration responses of the controlled and uncontrolled smart beams influenced by additive model uncertainty and a harmonic disturbance with a frequency of 2π rad/s: (a) sensor output, (b) control input.

optimized observer and DR control with GPI observer, the same controller gains are configured in the two DR control methods to analyze the influences of different observers on vibration suppression performance and robustness to model uncertainties.

In the first simulation, a harmonic disturbance with a frequency of 2π rad/s is applied and the maximum gain of the additive uncertainty is assumed to be 40% of the nominal system gain from control input to system output. The simulation results are displayed in Figures 5a and 5b, including the sensor and actuator voltages of uncontrolled smart beam, controlled smart beams using DR control with GPI observer not considering additive model uncertainty (DR-GPI), DR control with GPI observer considering additive model uncertainty (DR-GPI Uncertainty), DR control with H_∞ optimized observer not considering additive model uncertainty (DR-Hinf) and DR control with H_∞ optimized observer considering additive model uncertainty (DR-Hinf Uncertainty). It can be seen from Figure 5a that both two DR control methods can suppress vibration successfully and the DR control with H_∞ optimized observer has fast convergence speed. When additive uncertainty is considered in the simulation, the convergence speed of DR control with GPI observer clearly slows down. On the other hand, the sensor voltage

of DR control with H_∞ optimized observer shows no visible difference whether additive uncertainty is considered or not, which means robustness of the closed-loop system.

In the second simulation, a harmonic disturbance with the first eigenfrequency of the smart beam is applied. Since the closed-loop system of the smart beam is very sensitive at its first eigenfrequency, the maximum gain of the additive model uncertainty considered here is adjusted to 10% of the nominal system gain from control input to system output. Besides, to keep enough robustness of the controller, lower controller gains are configured in this simulation, which leads to smaller control input, i.e. the actuator voltage. The simulation results can be found in Figures 6a and 6b, which contains the sensor and actuator voltages of controlled and uncontrolled smart beams with additive model uncertainty considered and not considered. As shown in Figure 6a, it is clear that the DR control with H_∞ optimized observer can successfully suppress the vibration of the smart beam with or without additive model uncertainty. However, the DR control with GPI observer becomes divergent when there is additive model uncertainty in the system, which is mainly because the GPI observer is not robust enough to additive uncertainty, given the fact that the same gain is used in the controllers of the two DR control methods.
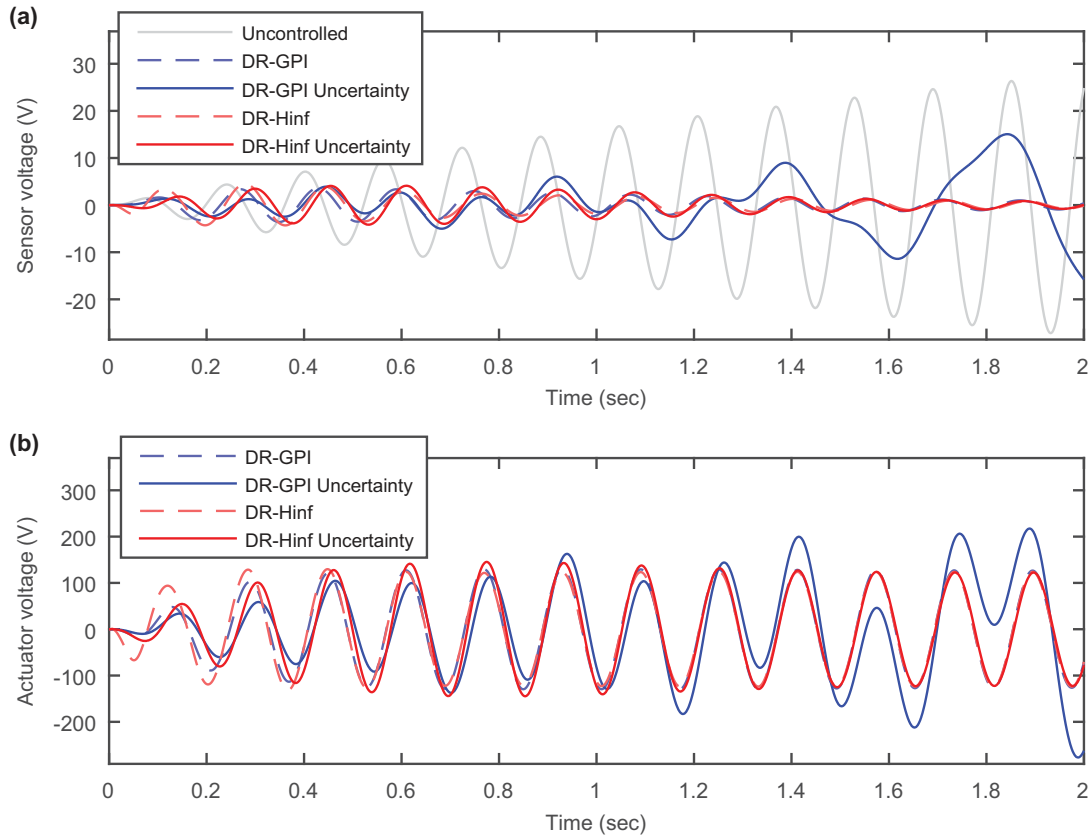
Fig. 6. The vibration responses of the controlled and uncontrolled smart beams influenced by additive model uncertainty and a harmonic disturbance with the first eigenfrequency of the smart beam: (a) sensor output, (b) control input.

4.2.2 Vibration suppression with measurement noise

In ideal situations where measurement noise is absent, the convergence speed is positively correlated with the observer gains. However, for the state space model of the second-order dynamic system in equation (5), the state variables of its state space system are composed of the displacement vector $\mathbf{q}$ and its derivative $\dot{\mathbf{q}}$, which makes the observer asymptotically approach a differentiator as the observer gains grow to infinity [52]. Therefore, the high-frequency measurement noise can be amplified enormously in a high-gain observer, which leads to corruption of the observed signals and a non-convergent closed-loop system. In the following two simulations, a Gaussian white noise with 1% peak value of the system output signal is considered as measurement noise, and a DR control with high-gain PI observer [42,53] is also implemented for comparison.

Similarly, two harmonic disturbances with a low frequency at 2π rad/s and the first eigenfrequency of the smart beam are applied in the following two simulations, respectively. The simulation results are shown in Figures 7a, 7b and Figures 8a, 8b, including the sensor and actuator voltages of uncontrolled smart beam, controlled smart beams using DR control with high-gain PI observer not considering measurement noise (DR-HGPI), DR control with high-gain PI observer considering measurement noise (DR-HGPI Noise), DR control with H_{∞} optimized observer not considering measurement noise (DR-Hinf) and DR control with H_{∞} optimized observer considering measurement noise (DR-Hinf Noise). When there is no noise in the system, the two DR control methods both suppress the vibration successfully. Due to the high feedback gains, the DR control with high-gain PI observer has faster response speed and performs better at the beginning of both two simulations. However, when measurement noise exists in the closed-loop system, the DR control with high-gain PI observer became divergent and the values of its sensor and actuator voltages just rocket up abnormally. On the other hand, the DR control with H_{∞} optimized observer is convergent and performs almost equally whether the measurement noise is considered or not. This is because the measurement noise is attenuated in the H_{∞} optimized observer, by setting the infinite norm of complementary sensitivity function small in high frequency range using properly configured weighting functions.
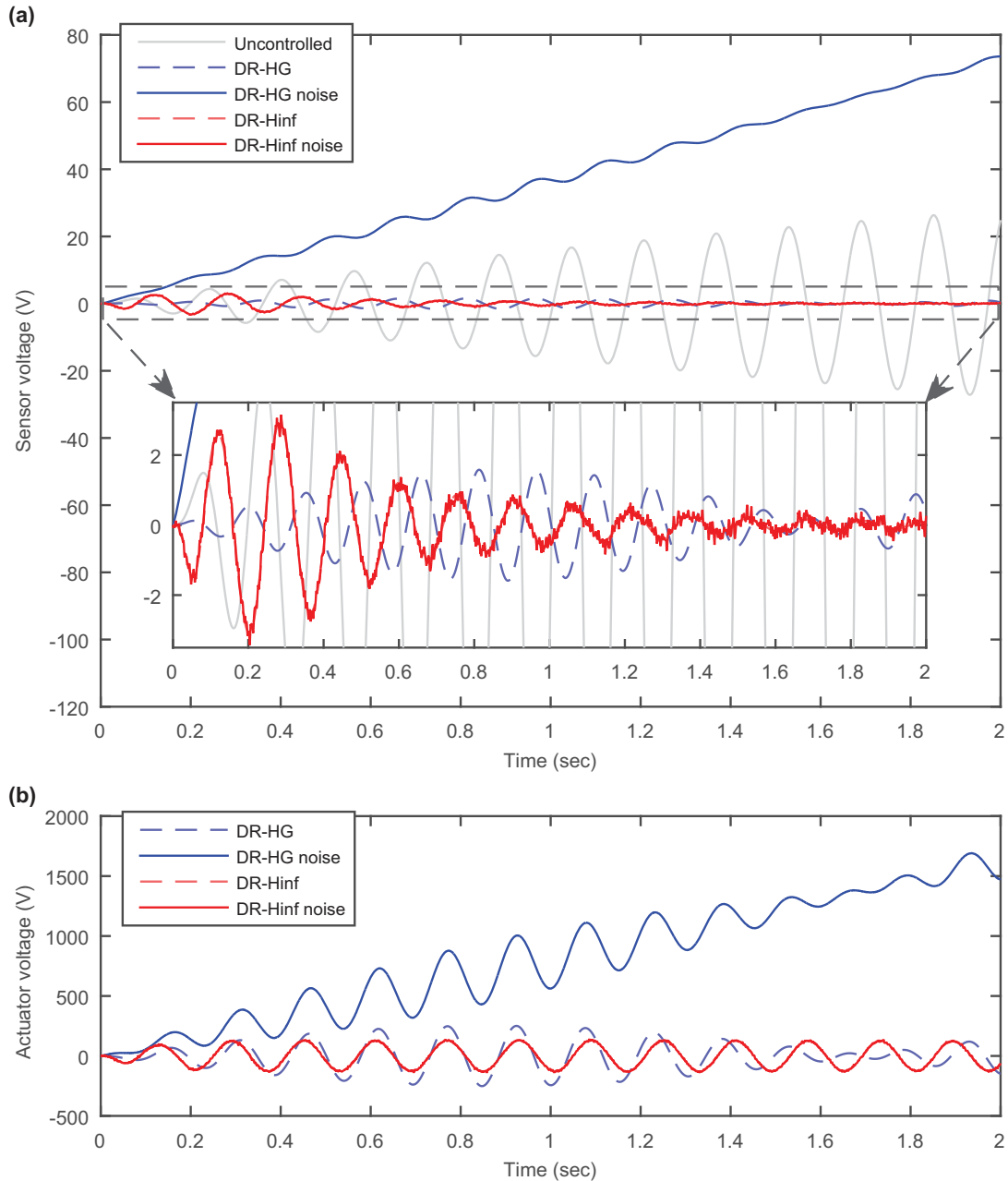
5 Conclusion

Aiming at suppressing vibrations of piezoelectric smart structures in the presence of model uncertainties and
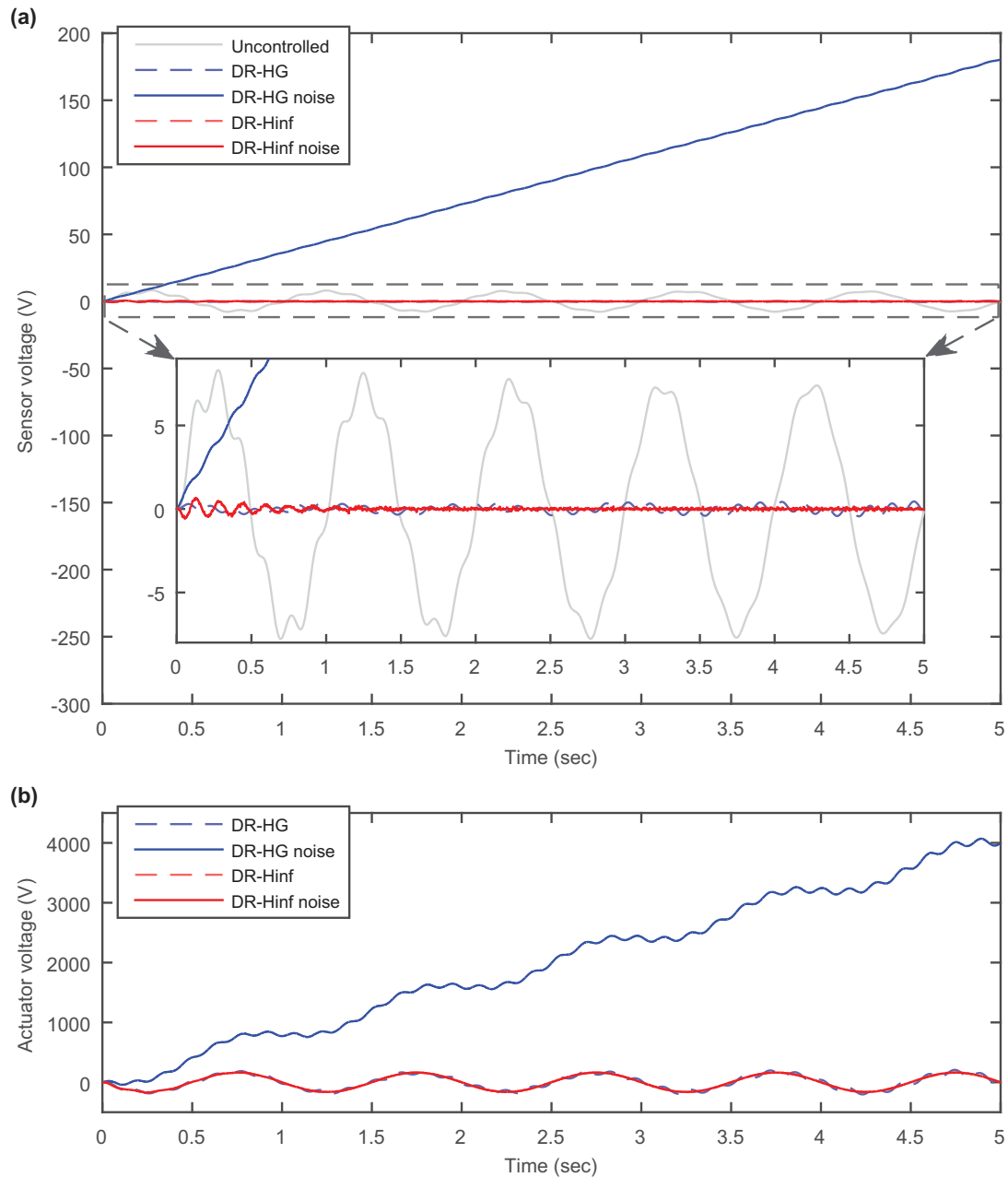
Fig. 7. The vibration responses of the controlled and uncontrolled smart beams influenced by measurement noise and a harmonic disturbance with a frequency of 2π rad/s: (a) sensor output, (b) control input.

measurement noise, a DR control with H_∞ optimized observer is developed in this paper. Based on FOSD hypothesis, the electro-mechanically coupled dynamic FE model of piezoelectric smart structures and the corresponding state space model are built. The state space model is extended by a fictitious disturbance model containing frequency information of disturbances. Based on the extended state space model, the H_∞ optimized observer is constructed with a dynamic feedback gain to estimate disturbances and state variables. The dynamic feedback gain of the observer is calculated by H_∞ mixed sensitivity optimization in which proper weighting func-

tions are selected to achieve desired response speed and robustness to model uncertainties and measurement noise. The estimated state variables and disturbances are fed back to the system through a conventional DR controller to form a stable closed-loop system and counteract disturbances. Vibration suppression simulations of a piezoelectric smart beam are implemented to validate the DR control with H_∞ optimized observer and compare with DR control with GPI observer and DR control with high-gain PI observer. It can be concluded from the simulation results that (i) in the absence of model uncertainties and measurement noise, the DR control with

Fig. 8. The vibration responses of the controlled and uncontrolled smart beams influenced by measurement noise and a harmonic disturbance with the first eigenfrequency of the smart beam: (a) sensor output, (b) control input.

H_∞ optimized observer has excellent vibration suppression performance which is similar to the other two DR control methods; (ii) in the presence of model uncertainties and measurement noise, the DR control with H_∞ optimized observer has better robustness than the other two DR control methods.

References

[1] U. Stöbener, L. Gaul, Active vibration control of a car body based on experimentally evaluated modal parameters, Mech. Syst. Signal Process. 15 (2001) 173–188

[2] M. Sabatini, P. Gasbarri, R. Monti, G.B. Palmerini, Vibration control of a flexible space manipulator during on orbit operations, Acta Astronaut. 73 (2012) 109–121

[3] Z. Wang, X. Qin, H.T.Y. Yang, Active suppression of panel flutter with piezoelectric actuators using eigenvector orientation method, J. Sound Vib. 331 (2012) 1469–1482

[4] X.Q. He, T.Y. Ng, S. Sivashanker, K.M. Liew, Active control of FGM plates with integrated piezoelectric sensors and actuators, Int. J. Solids Struct. 38 (2001) 1641–1655

[5] Y.K. Kang, H.C. Park, J. Kim, S.-B. Choi, Interaction of active and passive vibration control of laminated composite beams with piezoceramic sensors/actuators, Mater. Des. 23 (2002) 277–286

[6] J.M. Simões Moita, I.F.P. Correia, C.a.M. Mota Soares, C.A. Mota Soares, Active control of adaptive laminated structures with bonded piezoelectric sensors and actuators, Comput. Struct. 82 (2004) 1349–1358

[7] M.K. Kwak, S. Heo, Active vibration control of smart grid structure by multiinput and multioutput positive position feedback controller, J. Sound Vib. 304 (2007) 230–245

[8] J. Shan, H.-T. Liu, D. Sun, Slewing and vibration control of a single-link flexible manipulator by positive position feedback (PPF), Mechatronics 15 (2005) 487–503

[9] G. Song, S.P. Schmidt, B.N. Agrawal, Experimental robustness study of positive position feedback control for active vibration suppression, J. Guid. Control Dyn. 25 (2002) 179–182

[10] E. Omidi, S.N. Mahmoodi, Vibration control of collocated smart structures using H∞ modified positive position and velocity feedback, J. Vib. Control 22 (2016) 2434–2442

[11] H. Karagülle, L. Malgaca, H.F. Öktem, Analysis of active vibration control in smart structures by ANSYS, Smart Mater. Struct. 13 (2004) 661

[12] S.M. Khot, N.P. Yelve, R. Tomar, S. Desai, S. Vittal, Active vibration control of cantilever beam by using PID based output feedback controller, J. Vib. Control 18 (2012) 366–372

[13] S. Zhang, R. Schmidt, X. Qin, Active vibration control of piezoelectric bonded smart structures using PID algorithm, Chin. J. Aeronaut. 28 (2015) 305–313

[14] J. Fei, Active vibration control of flexible steel cantilever beam using piezoelectric actuators, in: Proceedings of the Thirty-Seventh Southeastern Symposium on System Theory, 2005, SSST '05, IEEE, NJ, 2005, pp. 35–39

[15] K. Makihara, J. Onoda, K. Minesugi, Using tuned electrical resonance to enhance bang-bang vibration control, AIAA J. 45 (2007) 497–504

[16] H.S. Tzou, W.K. Chai, Design and testing of a hybrid polymeric electrostrictive/piezoelectric beam with bang–bang control, Mech. Syst. Signal Process. 21 (2007) 417–429.

[17] Y. Wang, D.J. Inman, Comparison of control laws for vibration suppression based on energy consumption, J. Intell. Mater. Syst. Struct. 22 (2011) 795–809

[18] S. Narayanan, V. Balamurugan, Finite element modelling of piezolaminated smart structures for active vibration control with distributed sensors and actuators, J. Sound Vib. 262 (2003) 529–562

[19] M. Dadfarnia, N. Jalili, B. Xian, D.M. Dawson, A Lyapunov-based piezoelectric controller for flexible cartesian robot manipulators, J. Dyn. Syst. Meas. Control 126 (2004) 347–358

[20] E. Padoin, O. Menuzzi, E.A. Perondi, J.S.O. Fonseca, Modeling and LQR/LQG control of a cantilever beam using piezoelectric material, in: 22nd International Congress of Mechanical Engineering − COBEM, Vol. 2013, Ribeirao Preto, 2013, pp. 4629–4638

[21] C.M.A. Vasques, J. Dias Rodrigues, Active vibration control of smart piezoelectric beams: Comparison of classical and optimal feedback control strategies, Comput. Struct. 84 (2006) 1402–1414

[22] K.R. Kumar, S. Narayanan, Active vibration control of beams with optimal placement of piezoelectric sensor/actuator pairs, Smart Mater. Struct. 17 (2008) 055008

[23] W.P. Li, H. Huang, Integrated optimization of actuator placement and vibration control for piezoelectric adaptive trusses, J. Sound Vib. 332 (2013) 17–32

[24] J.W. Sohn, S.-B. Choi, H.S. Kim, Vibration control of smart hull structure with optimally placed piezoelectric composite actuators, Int. J. Mech. Sci. 53 (2011) 647–659

[25] Z.-G. Song, F.-M. Li, Optimal locations of piezoelectric actuators and sensors for supersonic flutter control of composite laminated panels, J. Vib. Control 20 (2014) 2118–2132

[26] S. Kapuria, M.Y. Yasin, Active vibration control of piezoelectric laminated beams with electroded actuators and sensors using an efficient finite element involving an electric node, Smart Mater. Struct. 19 (2010) 045019

[27] S.B. Choi, J.W. Sohn, Chattering alleviation in vibration control of smart beam structures using piezofilm actuators: experimental verification, J. Sound Vib. 294 (2006) 640–649

[28] Z.-C. Qiu, J.-D. Han, X.-M. Zhang, Y.-C. Wang, Z.-W. Wu, Active vibration control of a flexible beam using a non-collocated acceleration sensor and piezoelectric patch actuator, J. Sound Vib. 326 (2009) 438–455

[29] A.G. Wills, D. Bates, A.J. Fleming, B. Ninness, S.O.R. Moheimani, Model predictive control applied to constraint handling in active noise and vibration control, IEEE Trans. Control Syst. Technol. 16 (2008) 3–12

[30] R. Dubay, M. Hassan, C. Li, M. Charest, Finite element based model predictive control for active vibration suppression of a one-link flexible manipulator, ISA Trans. 53 (2014) 1609–1619

[31] M. Marinaki, Y. Marinakis, G.E. Stavroulakis, Fuzzy control optimized by a Multi-Objective Differential Evolution algorithm for vibration suppression of smart structures, Comput. Struct. 147 (2015) 126–137

[32] J.-J. Wei, Z.-C. Qiu, Y.-C. Wang, Experimental comparison research on active vibration control for flexible piezoelectric manipulator using fuzzy controller, J. Intell. Robot. Syst. 59 (2010) 31–56

[33] O. Abdeljaber, O. Avci, D.J. Inman, Active vibration control of flexible cantilever plates using piezoelectric materials and artificial neural networks, J. Sound Vib. 363 (2016) 33–53

[34] R. Kumar, S.P. Singh, H.N. Chandrawat, MIMO adaptive vibration control of smart structures with quickly varying parameters: neural networks vs classical control approach, J. Sound Vib. 307 (2007) 639–661

[35] Z. Qiu, X. Zhang, C. Ye, Vibration suppression of a flexible piezoelectric beam using BP neural network controller, Acta Mech. Solida Sin. 25 (2012) 417–428

[36] S. Li, J. Qiu, H. Ji, K. Zhu, J. Li, Piezoelectric vibration control for all-clamped panel using DOB-based optimal control, Mechatronics 21 (2011) 1213–1221

[37] J. Han, From PID to active disturbance rejection control, IEEE Trans. Ind. Electron. 56 (2009) 900–906

[38] S. Li, J. Li, Y. Mo, Piezoelectric multimode vibration control for stiffened plate using ADRC-based acceleration compensation, IEEE Trans. Ind. Electron. 61 (2014) 6892–6902

[39] S. Li, J. Li, Y. Mo, R. Zhao, Composite multi-modal vibration control for a stiffened plate using non-collocated acceleration sensor and piezoelectric actuator, Smart Mater. Struct. 23 (2014) 015006

[40] Z. Gao, Scaling and bandwidth-parameterization based controller tuning, in: Proceedings of the American Control Conference, 2003, Vol. 6, IEEE, NJ, 2003, pp. 4989–4996.

[41] P.C. Müller, J. Lückel, Optimal multivariable feedback system design with disturbance rejection, Probl. Control Inf. Theory 6 (1977) 211–227

[42] S.Q. Zhang, H.N. Li, R. Schmidt, P.C. Müller, Disturbance rejection control for vibration suppression of piezoelectric laminated thin-walled structures, J. Sound Vib. 333 (2014) 1209–1223

[43] S.-Q. Zhang, R. Schmidt, P.C. Müller, X.-S. Qin, Disturbance rejection control for vibration suppression of smart beams and plates under a high frequency excitation, J. Sound Vib. 353 (2015) 19–37

[44] S.Q. Zhang, R. Schmidt, Large rotation FE transient analysis of piezolaminated thin-walled smart structures, Smart Mater. Struct. 22 (2013) 105025

[45] S.-Q. Zhang, Y.-X. Li, R. Schmidt, Modeling and simulation of macro-fiber composite layered smart structures, Compos. Struct. 126 (2015) 89–100

[46] S.Q. Zhang, R. Schmidt, Static and dynamic FE analysis of piezoelectric integrated thin-walled composite structures with large rotations, Compos. Struct. 112 (2014) 345–357

[47] J. Doyle, K. Glover, P. Khargonekar, B. Francis, State-space solutions to standard H2 and H∞ control problems, in: 1988 American Control Conference, 1988, pp. 1691–1696

[48] D. Xue, Y. Chen, D.P. Atherton, Linear feedback control: analysis and design with MATLAB, SIAM, Philadelphia, 2007

[49] A.E. Bryson, Y.C. Ho, Applied optimal control: optimization, estimation, and control, Taylor & Francis, Bristol, 1975

[50] S. Marburg, Six boundary elements per wavelength: Is that enough? J. Comput. Acoust. 10 (2002) 25–51

[51] P. Langer, M. Maeder, C. Guist, M. Krause, S. Marburg, More than six elements per wavelength: the practical use of structural finite element models and their accuracy in comparison with experimental results, J. Comput. Acoust. 25 (2017) 1750025

[52] H.K. Khalil, Analysis of sampled-data high-gain observers in the presence of measurement noise, Eur. J. Control 15 (2009) 166–176

[53] Y. Liu, D. Söffker, Variable high-gain disturbance observer design with online adaption of observer gains embedded in numerical integration, Math. Comput. Simul. 82 (2012) 847–857